

# SECOND ORDER MODELLING OF COMPOUND OPEN-CHANNEL FLOWS

Olfa DABOUSSI <sup>(1)</sup>, Zouhaier HAFSIA <sup>(2)</sup> and Mahmoud MOUSSA <sup>(3)</sup>  
<sup>(1-3)</sup> *ENIT. Laboratoire d'Hydraulique B.P. 37. Le Belvédère, 1002 Tunis, Tunisia*

E-mail : <sup>(2)</sup> [Zouhaier.Hafsia@enit.rnu.tn](mailto:Zouhaier.Hafsia@enit.rnu.tn)    <sup>(3)</sup> [Mahmoud.Moussa@enit.rnu.tn](mailto:Mahmoud.Moussa@enit.rnu.tn)

## **ABSTRACT**

The aim of the present work is to determine the secondary currents structure in a compound channel flow. We have tested two turbulence models based on one point closure. The first order k- $\epsilon$  model and the second order Reynolds stress model. The numerical simulations of the transport equations is realised by the computational fluid dynamic code PHOENICS which integrates these two turbulence model.

Numerical simulations show that the k- $\epsilon$  model can not reproduce the secondary currents. The Reynolds stress turbulence model is therefore necessary to reproduce the flow structure. The secondary currents affected the main velocity, kinetic energy and turbulent intensities distributions. This effect is shown by the isovalues bulging in the vicinity of the main channel floodplain interface. These bulges are due to the secondary convection that expressed the momentum transfer on the main channel flood plain interface. The momentum transfer is quantified by the apparent shear stress. The secondary currents structure is affected by the relative depth variation. In fact, the free surface vortex disappears when relative depth drops. These interpretations refer to the three-dimensional nature of the flow.

The three-dimensional study has allowed to evaluate the dispersion coefficient  $\alpha$  which appears in the integrated 1D models. In the fluvial hydraulic,  $\alpha$  is equal to 1. Calculations show that  $\alpha$  is really different from the 1 and it is dependent to the relative depth through a polynomial relation.

## **1- INTRODUCTION**

After a strong rain for a long time, the floods occur and generates an increasing of the water level and overbanks. Water level can reach the areas around the river which can be agriculture zones, forest, habitation or other. This emphasises the need of more accurate predictions of river flood levels and required advanced studies of the elementary phenomena that governs the river flow.

The river with it's floods regions constitute a compound channel. The compound channel is composed by two elements, the main channel that contains the permanent and faster flow, and the floodplain which is often shallow and where there is a slowly flow. In nature, the compound channel is formed by many intermediate stages between main channel and flood plain and are not easy to reproduce because of their variability. So, laboratory researches and numerical simulations use elementary forms : rectangular or trapezoidal. In the case of a rectangular compound channel flow we note a strong shear stress on the main channel – flood plain junction. It is governed by the mechanism of secondary currents. These are expressed by

two vortexes : the main channel one and the free surface one. This gives to the flow a three-dimensional structure.

The researches about the compound channel flows is wide and concerned one, two and three dimensional flow. The one dimensional studies are empirical and have as objective to correct classical discharge formulae. We can mention the works of Knight and Demetriou (1983), Myers (1987), Shino and Knight (1991), Myers and al. (2001), Seckin (2004) and others. But these studies do not give information about the flow structure which require a three dimensional flow analysis with an appropriate turbulence model. In the case of a Newtonian fluid and a parabolic flow, the first order model k-ε based on the isotropic approximation of Boussinesq can not determine the secondary currents structure near the separation region between main channel and flood plains. Hence, some researchers developed the non linear k-ε model for high Reynolds number (Pezzinga, 1994) and low Reynolds number (Sofialidis and Prinos, 1998). But a few works treated the second order model RSM (Reynolds stress model) as the study of Krishnappan and Lau (1986) who use an algebraic Reynolds stress model. Cokljat and Younis (1995) have applied the full Reynolds stress model; they validate their numerical simulations with the experimental data of Tominaga and al. (1989). The simulation showed that the Reynolds stress model can reproduce the anisotropy of flow, especially near the interface.

In this work we propose to apply the Reynolds stress model (RSM) in order to reproduce momentum transfer representing the interaction between the main channel and floodplain interaction in the case of a rectangular open compound channel flow. The tested  $R_{ij}$  model is developed by Launder and al. (1975) and it is integrated in the CFD code PHOENICS. The validation data is those of Tominaga and al. (1989). The simulation results show that the dispersion coefficient vary in function of the relative depth for the same width parameter.

## 2- GOVERNING EQUATIONS

### 2-1 Transport equations

In the case of a stationary ( $\frac{\partial}{\partial t} = 0$ ) and parabolic (derivation through z direction is zero) flow and a Newtonian fluid with constant viscosity, the Reynolds averaged Navier-Stokes equations are written in Cartesian tensor as following (Schiestel, 1993) :

- Continuity equation :

$$\frac{\partial}{\partial x_i} (r \bar{U}_i) = 0 \quad (1)$$

- Reynolds average transport momentum equation :

$$\frac{\partial}{\partial x_i} (r \bar{U}_i \bar{U}_j) = - \frac{\partial \bar{P}}{\partial x_j} + r n \frac{\partial^2 \bar{U}_i}{\partial x_i \partial x_j} - \frac{\partial}{\partial x_i} (r \overline{u'_i u'_j}) + r \underbrace{g_i}_V \quad (2)$$

I : Convective transfer;

II : Pressure gradient;

III : Diffusion due to molecular viscosity;

IV : Diffusion due to the Reynolds stresses;

V : Gravity field.

The unknown  $-\overline{r u'_i u'_j} = t_{ij}$  is expressed by the Reynolds stress transport equation which is written in tensorial notation as :

$$\overline{U}_m \frac{\partial t_{ij}}{\partial x_m} = D_{ij} + P_{ij} - e_{ij} + Q_{ij} \quad (3)$$

The  $D_{ij}$  expressed the diffusivity of Reynolds stresses by the velocity fluctuation. This term is expressed by the model of Daly-Harlow (Banjac and Vasiljevic, 2004) :

$$D_{ij} = -\frac{\partial}{\partial x_m} \left( C_s \frac{k}{re} t_{mn} \frac{\partial t_{ij}}{\partial x_n} \right) \quad (4)$$

$C_s$  is an empirical constant.

The production  $P_{ij}$  does not need to be modelled, the expression is :

$$P_{ij} = -(t_{im} \frac{\partial \overline{U}_j}{\partial x_m} + t_{jm} \frac{\partial \overline{U}_i}{\partial x_m}) \quad (5)$$

The destruction  $e_{ij}$  is modelled assuming the local isotropy :

$$e_{ij} = -\frac{2}{3} re d_{ij} \quad (6)$$

The last term  $Q_{ij}$  expresses the pressure-strain correlation is modelled through the sum of two part  $Q_{ij}^1$  and  $Q_{ij}^2$ . The first part  $Q_{ij}^1$  is the slow pressure-strain correlation. It is composed to the slow correlation ( $Q_{ij}^{1'}$ ) and the wall reflection correction ( $Q_{ij}^{w1}$ ).

The second part is the rapid pressure-strain correlation which is also composed to two parts the main term ( $Q_{ij}^{2'}$ ) and the wall reflection correction ( $Q_{ij}^{w2}$ ).

Launder and al., expressed  $Q_{ij}^{1'}$  by :

$$Q_{ij}^{1'} = -C_1 \frac{e}{k} (t_{ij} + \frac{2}{3} d_{ij} r k) \quad (7)$$

$C_1$  is an empirical constant.

The wall reflection corrective term of the slow pressure-strain correlation is :

$$Q_{ij}^{w1} = C_{w1} \frac{e}{k} f_w (t_{km} n_k n_m d_{ij} - \frac{3}{2} t_{ki} n_k n_j - \frac{3}{2} t_{kj} n_k n_i) \quad (8)$$

$f_w$  is the wall dumping function  $f_w = C_w \frac{1}{y_n}$ ,  $y_n$  is the normal distance from the wall.  $l$  is the

turbulence length scale  $l = C_D \frac{k^{3/2}}{\epsilon}$ ,  $C_D$  is constant.  $C_w$  is function of the near wall grid point

$$y_{nw} : C_w = \frac{y_{nw}}{l}$$

The second part of the pressure-strain correlation or the rapid correlation  $Q_{ij}^{2'}$  is modelled by four methods : the quasi-isotropic model (QI), the isotropisation of production (IPM), the (IP) of Younis and the (SSG) model. These turbulence model closure are integrated in the PHOENICS code. In this work, we have applied the (IP) model of Launder and al.. So, the  $Q_{ij}^{2'}$  is modeled as :

$$Q_{ij}^{2'} = -C_2 (P_{ij} - \frac{1}{3} d_{ij} P_{kk}) \quad (9)$$

$P_{ij}$  is the stress production.

The second wall reflection correction term for the rapid part is :

$$Q_{ij}^{w2} = C_{w2} f_w (Q_{km}^{2'} n_k n_m d_{ij} - \frac{3}{2} Q_{ki}^{2'} n_k n_j - \frac{3}{2} Q_{kj}^{2'} n_k n_i) \quad (10)$$

The RSM model require the averaged equation of the turbulent kinetic equation and the dissipation rate  $\epsilon$ . The corresponding transport equations of  $k$  and  $\epsilon$  are :

- Turbulent kinetic energy equation k :

$$\overline{U}_i \frac{\partial k}{\partial x_i} = \frac{\partial}{\partial x_i} \left( \overline{n}_i \frac{\partial k}{\partial x_i} \right) - \overline{u'_i u'_j} \frac{\partial \overline{U}_i}{\partial x_j} - \overline{e} \quad (11)$$

I : Convection of k;

II : Diffusion;

III : Production;

IV : Dissipation.

- Dissipation rate equation  $\varepsilon$  :

$$\frac{\partial}{\partial x_i} (\overline{r U}_i \varepsilon) = - \frac{\partial}{\partial x_i} (C_e \frac{k}{e} t_{ij} \frac{\partial \varepsilon}{\partial x_j}) + r \frac{e}{k} (\frac{1}{2} C_{e1} P_{kk} - C_{e2} e) \quad (12)$$

I : Convection of  $\varepsilon$ ;

II : Diffusion;

III : (Production) – (Destruction).

The following table shows the values of the empirical constants.

**Table 1: Empirical constants values (Banjac and Vasiljevic, 2004)**

$C_s$	$C_1$	$C_2$	$C_{w1}$	$C_{w2}$	$C_D$	$C_\mu$	$C_\varepsilon$	$C_{\varepsilon 1}$	$C_{\varepsilon 2}$
0.22	1.80	0.60	0.50	0.30	0.13	0.50	0.80	1.45	1.90

## **2-2 Boundary conditions**

Near the wall, the velocity is represented by the logarithmic wall law :

$$\overline{U}^+ = \frac{1}{\kappa} \ln(y^+ E) \quad (13)$$

$\overline{U}^+ = \frac{\overline{U}}{U_*}$ ,  $y^+ = \frac{U_* y}{\nu}$  ( $30 < y^+ < 100$ ) and E is the roughness constant equal to 8.6.

In addition, the appropriate wall shear stresses is set equal to zero.

The free surface is considered as a symmetric plane (Krishnappan and Lau, 1986).

The inlet conditions imposed are :

$$* k_{in} = (I W_{in})^2 ; I = \frac{\sqrt{\overline{u'^2} + \overline{v'^2} + \overline{w'^2}}}{\sqrt{\overline{U}^2 + \overline{V}^2 + \overline{W}^2}}, \text{ the turbulent intensity.} \quad (14)$$

$$* \varepsilon_{in} = \frac{0.1643 k_{in}^{1.5}}{l_m} ; l_m \text{ is 1\% of the hydraulic radius.} \quad (15)$$

$$* \text{ The normal Reynolds stresses are : } \overline{u'^2} = \overline{v'^2} = \overline{w'^2} = \frac{2}{3} k_{in} \quad (16)$$

\* The tangential Reynolds stresses are zero.

## **3- NUMERICAL SIMULATIONS**

### 3-1 Tested cases

The experimental data presents three cases of the relative depth  $\beta$  ( $\beta = \frac{H-h}{H}$ , ( $H-h$ ) is the flood plain depth and  $H$  is the total depth) and for constant  $\lambda$  (the width parameter  $\lambda = \frac{B}{b}$ ,  $B$  the total width and  $b$  the width of the main channel) (fig. 1). The following table contains the geometrical and experimental conditions.

**Table 2 : Data of Tominaga and al. (1989)**

Case	B (m)	b (m)	$\lambda = B/b$	h (m)	H (m)	$\beta = (H-h)/H$	$W_{moy}$ ( $m s^{-1}$ )
1	0.195	0.094	2.07	0.0501	0.1001	0.500	0.315
2	0.195	0.094	2.07	0.0501	0.0661	0.242	0.320
3	0.195	0.094	2.07	0.0501	0.0763	0.343	0.273

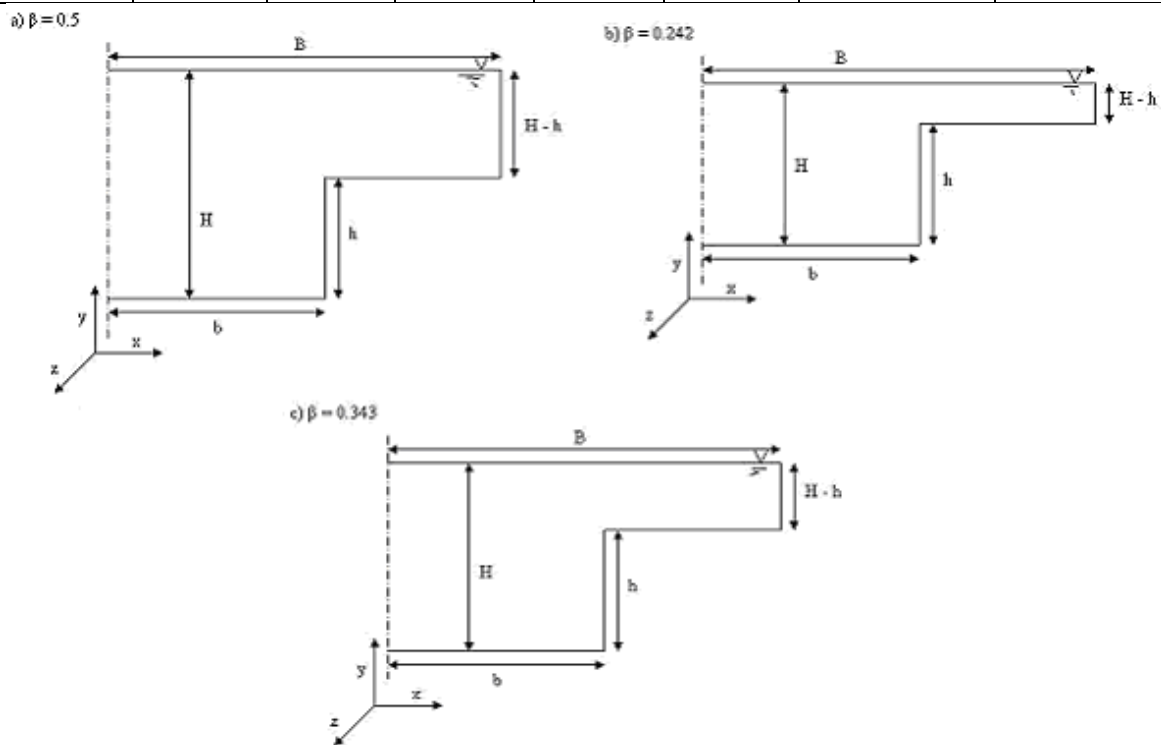


**Figure 1 : Tested cases**

For a developed flow, the flow field depends only on  $x$  and  $y$  directions. So, the grid is composed with meshes of different sizes in this plane. The numerical scheme used by PHOENICS code is the finite volume method. The following table and figure summarise the grid dimensions for each case.

**Table 2 : Grid dimensions**

	Zone I		Zone II		Zone III	
	$\Delta x$ (m)	$\Delta y$ (m)	$\Delta x$ (m)	$\Delta y$ (m)	$\Delta x$ (m)	$\Delta y$ (m)
Coarse grid	$b/10$	$h/10$	$b/10$	$(H-h)/10$	$(B-b)/16$	$(H-h)/10$
Thin grid	$b/30$	$h/18$	$b/30$	$(H-h)/38$	$(B-b)/68$	$(H-h)/38$

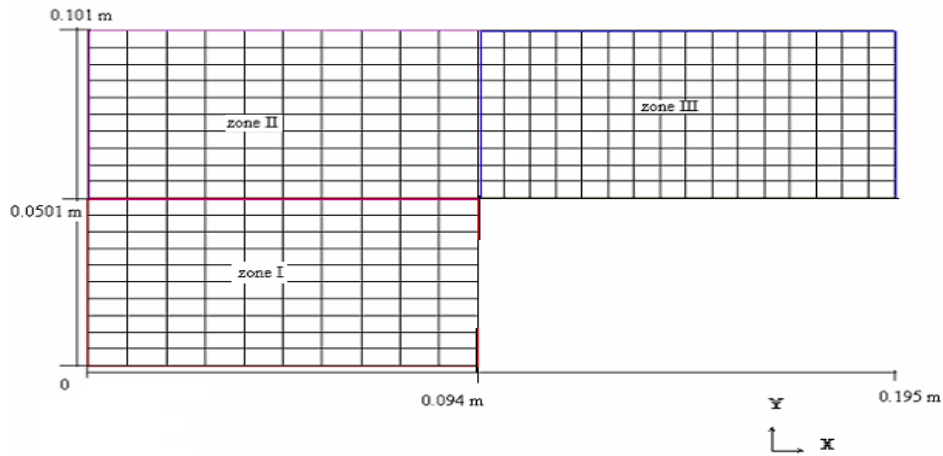


**Figure 2 : The grid repartition**

### **3-2 First order turbulence model**

The fig. 3 show the main velocity variation ( $\frac{\overline{W}}{W_{max}}$ ) in the case of  $\beta = 0.5$  when we apply a k- $\epsilon$  turbulence model. Numerical simulations show that the k- $\epsilon$  model can not reproduce the isovalues bulging in the vicinity of the main channel - floodplain interface (figure 3).

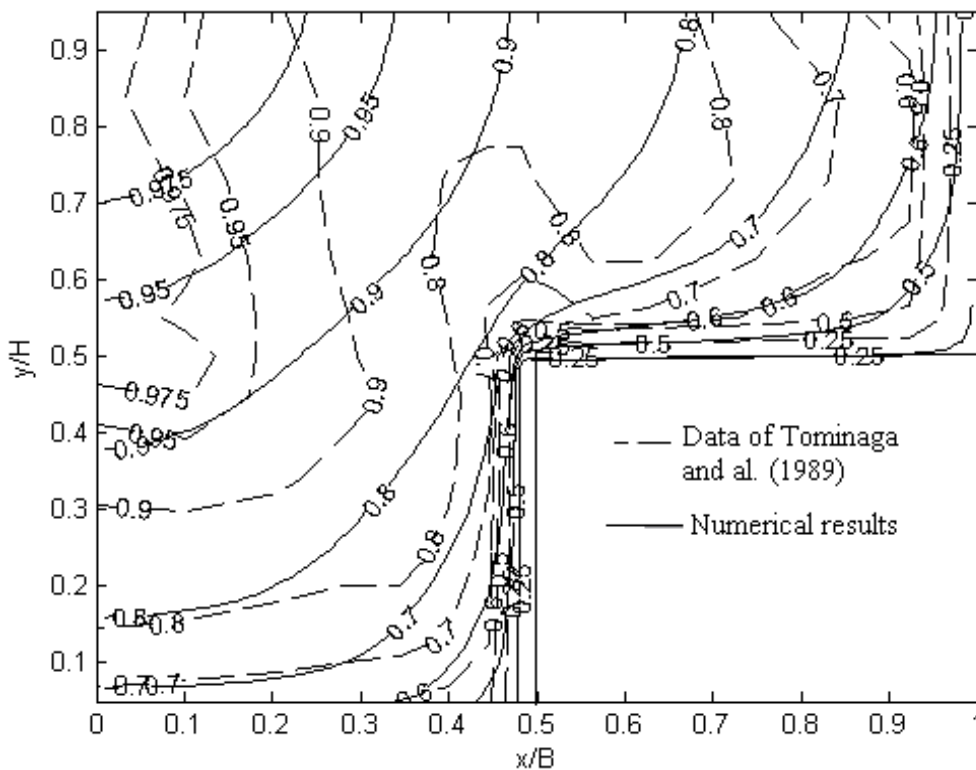


**Figure 3 : Secondary currents in the case of  $\beta = 0.5$  (numerical and experimental data)**

In order to reproduce the secondary currents structure we use the second order turbulence model (RSM) and we in present the following the corresponding results.

### **3-3 Secondary currents**

They are characterised by the presence of two vortices near the junction between main channel and floodplain for the  $\beta = 0.5$ . The numerical results obtained by RSM model are in accordance with the experimental data of Tominaga and al. (1989) (fig. 4).

The secondary currents structure is affected by the relative depth variation (fig. 5 and 6). Their intensity rises when  $\beta$  decreases.

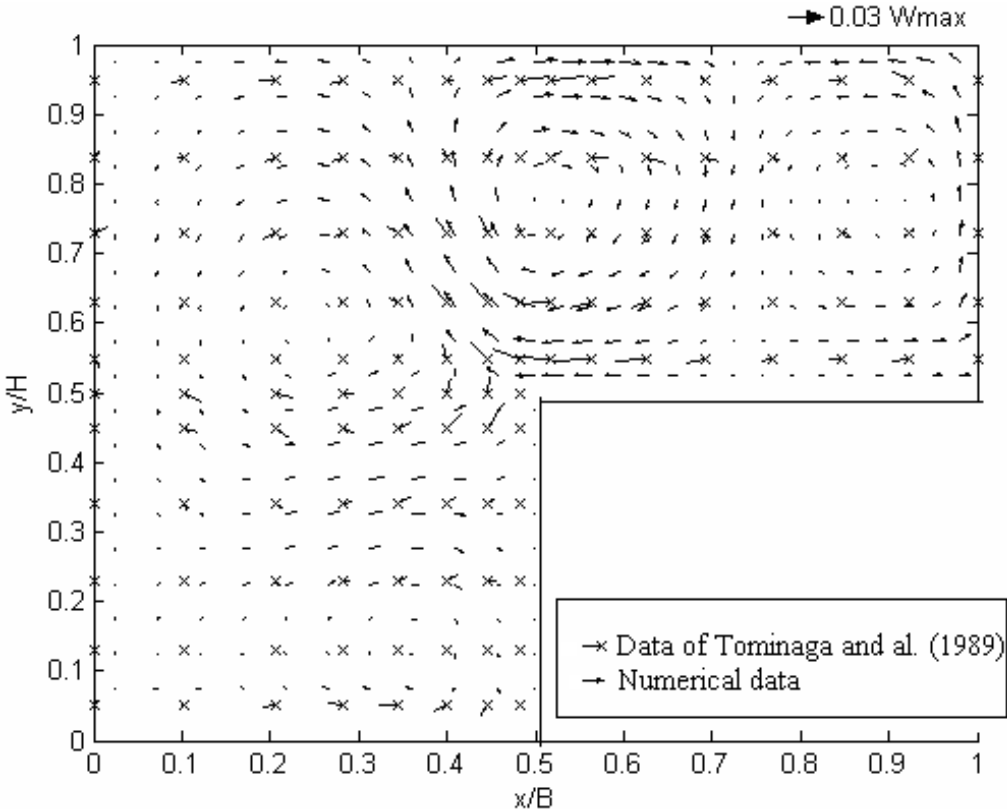


Figure 4 : Secondary currents in the case of  $\beta = 0.5$  (numerical and experimental data)

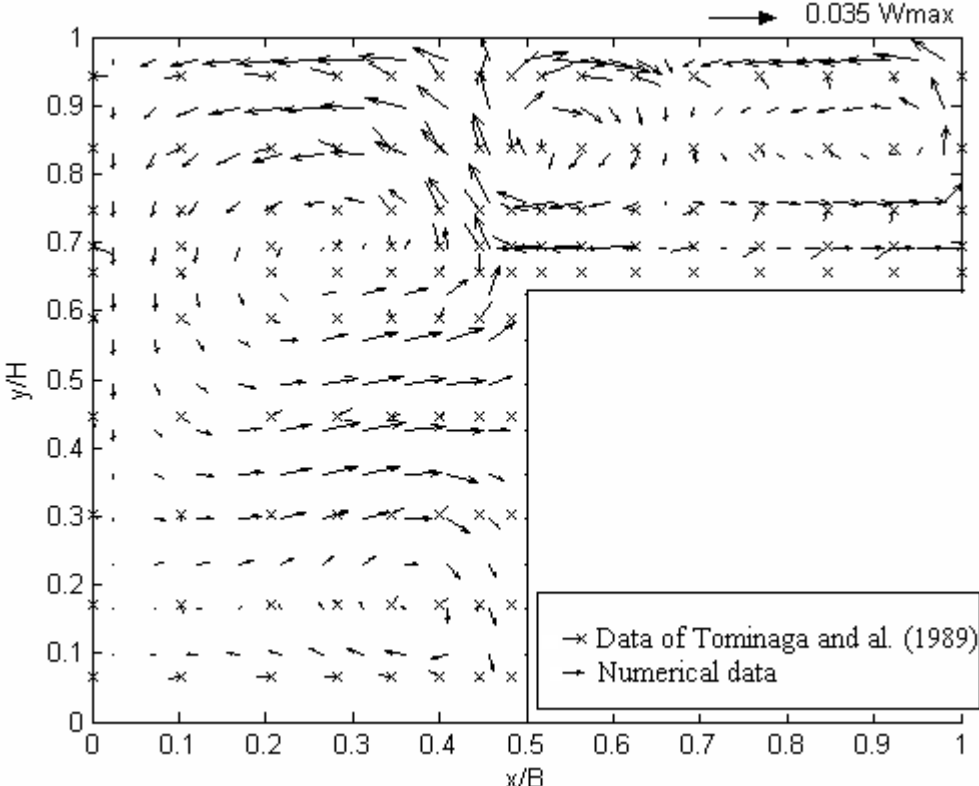
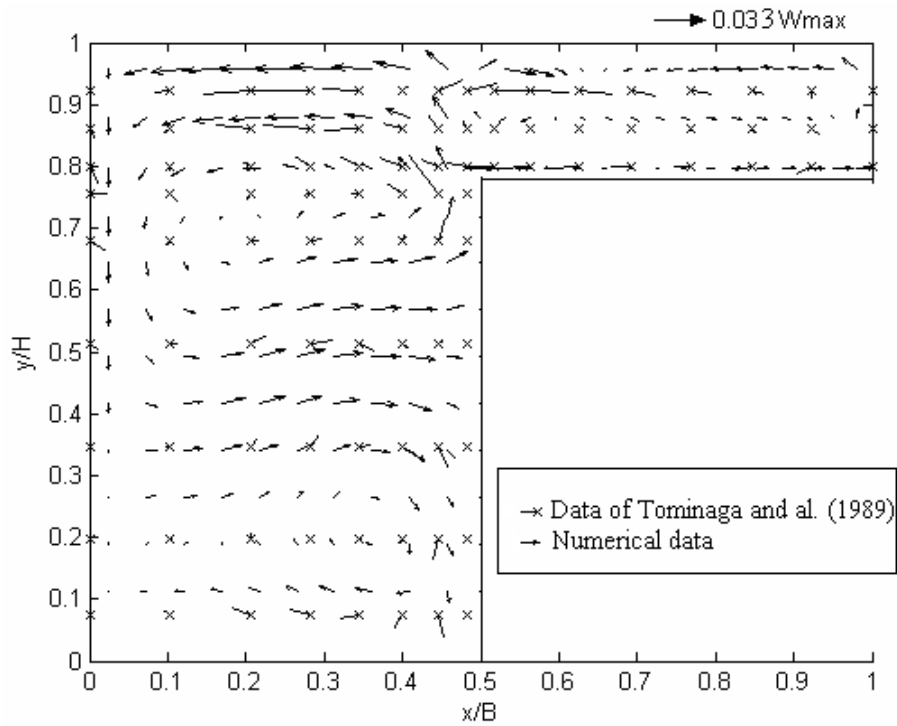


Figure 5 : Secondary currents in the case of  $\beta = 0.343$  (numerical and experimental data)



**Figure 6 : Secondary currents in the case of  $\beta = 0.242$  (numerical and experimental data).**

### 3-4 Main velocity variation

The fig. 7, 8 and 9 show the main velocity variation in the case of  $\beta = 0.5$ ; 0.343 and 0.242. The isovelocity  $\frac{\bar{W}}{W_{max}}$  bulges near the junction towards the free surface within the inclined plan beginning from the junction and finished near the free surface. The bulging effects are decreased when  $\beta$  diminished. The bulgings are due to the secondary flow near the junction.

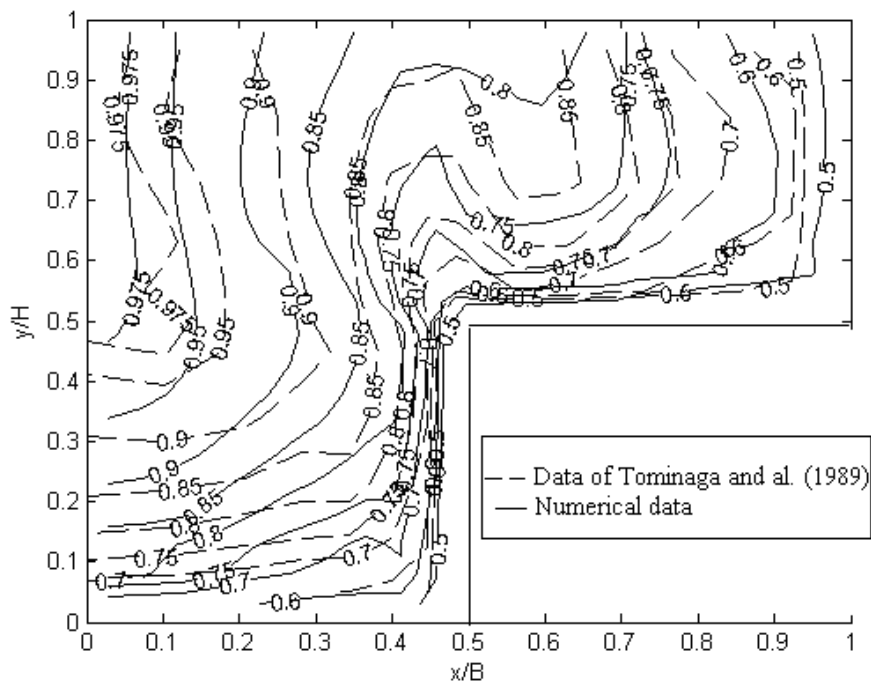


**Figure 7 : Numerical iso-velocity  $\frac{\bar{W}}{W_{max}}$  compared to Tominaga and al. (1989):  $\beta = 0.5$ .**

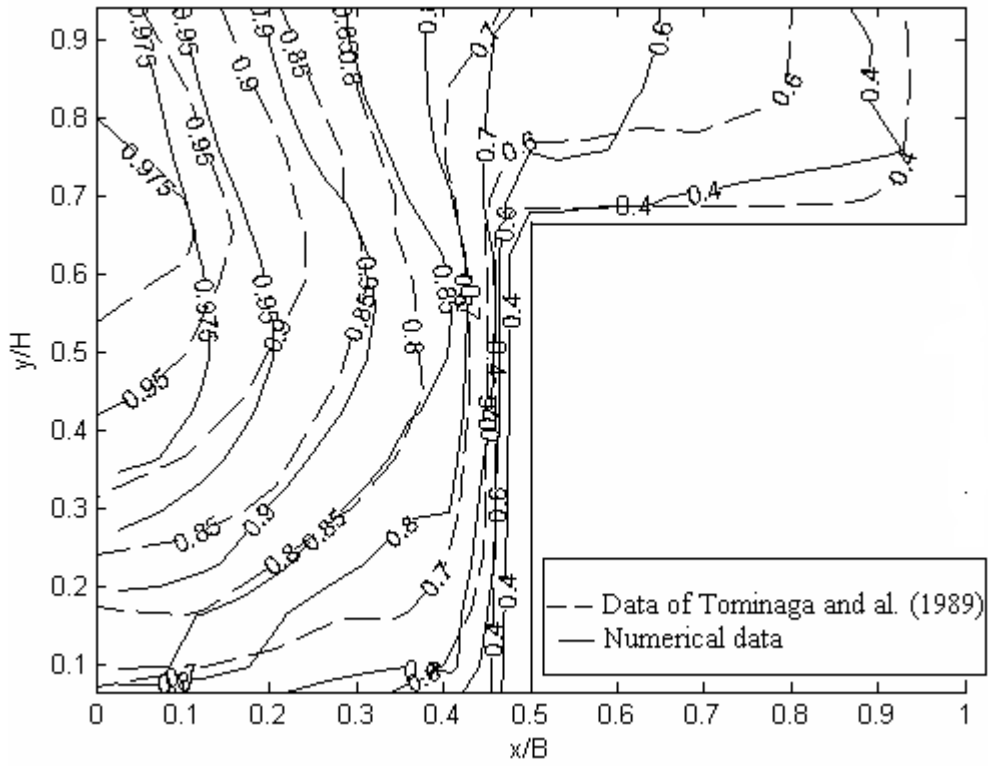


Figure 8 : Numerical iso-velocity  $\frac{\bar{W}}{W_{\max}}$  compared to Tominaga and al. (1989):  $\beta = 0.343$ .

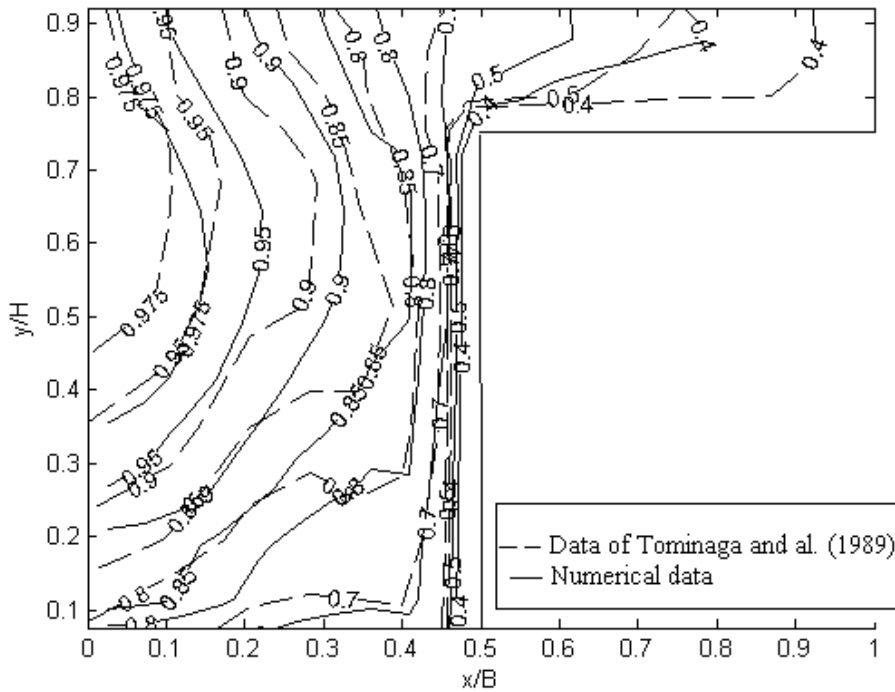
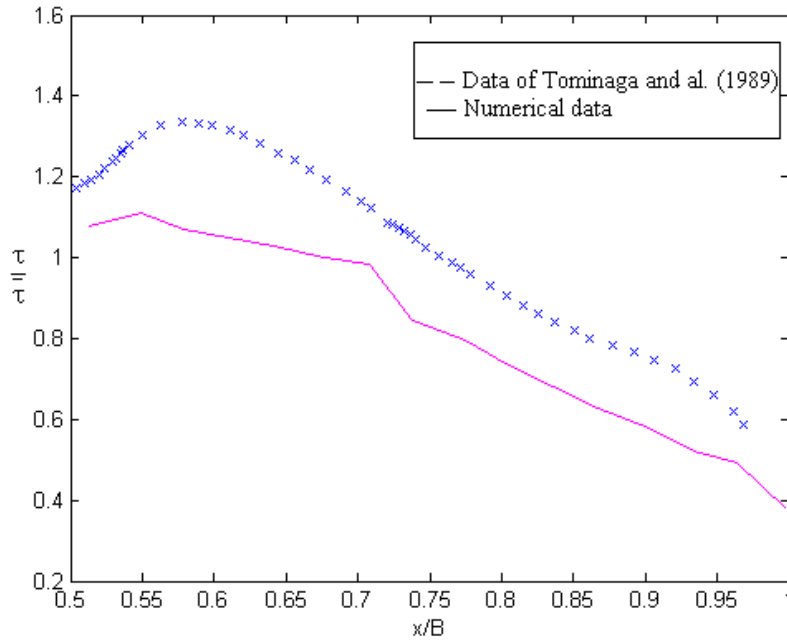


Figure 9 : Numerical iso-velocity  $\frac{\bar{W}}{W_{\max}}$  compared to Tominaga and al. (1989):  $\beta = 0.242$ .

### 3-5 Wall shear stress

The figure 10 shows the variation of  $t/\bar{t}$  on the floodplain where  $\tau = \rho U_*$  is the shear stress on the floodplain ( $U_*$  is the friction velocity) and  $\bar{\tau} = \rho \bar{U}_*$  is the average shear stress ( $\bar{U}_*$  is the average friction velocity on the bed). The wall shear on the floodplain rises considerably near the junction. Figure 10 shows that numerical simulation underestimates them.



**Figure 10 : Shear wall in the floodplain bed ( $\beta = 0.5$ )**

### 3-6 Local velocity variation

The local velocity  $W_1$  profile is parabolic near the centre of the main channel (fig. 11). Near the junction, numerical results show that the velocity profile present same discontinuity near the wall (fig. 12). It turns to the parabolic form near the vertical wall of the floodplain (fig. 13).

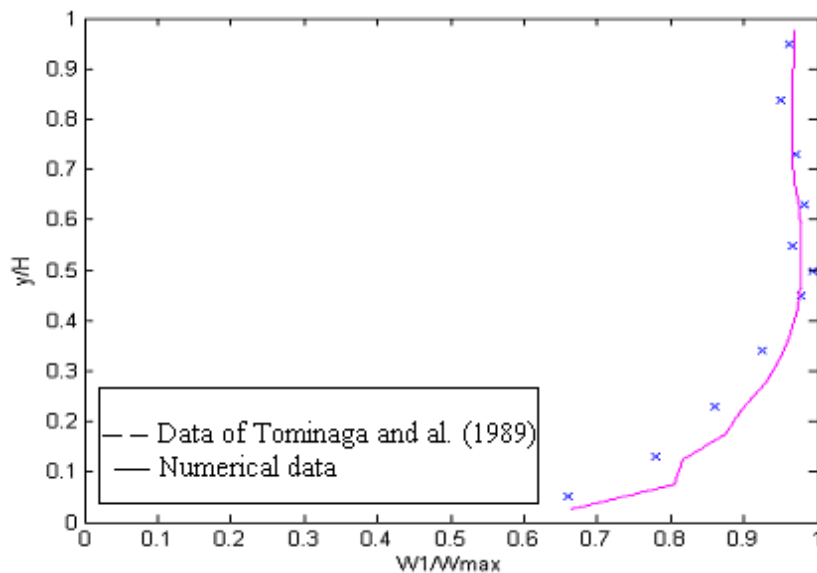


**Figure 11 : Velocity profile near the symmetric plane ( $\beta = 0.5$ )**

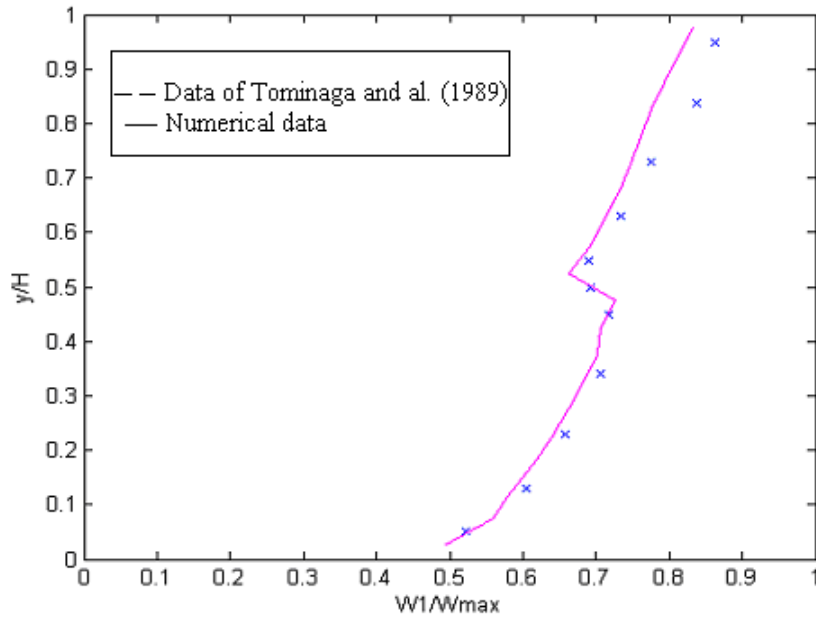


**Figure 12 : Velocity profile near the junction ( $\beta = 0.5$ )**

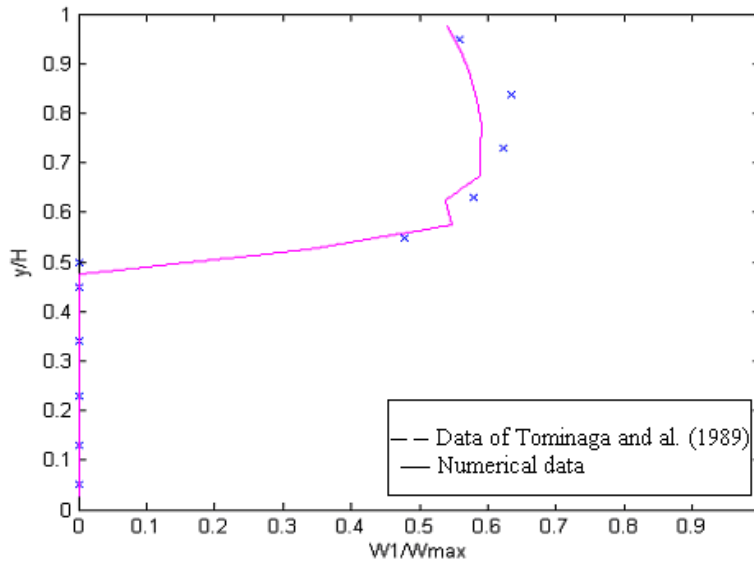


**Figure 13 : Velocity profile near the vertical wall of the floodplain ( $\beta = 0.5$ )**

The comparison of numerical simulation with the data of Tominaga and al. (1989) proves that the CFD code PHOENICS gives acceptable results. So, we are used to check the coefficient dispersion value appeared in the integrated models.

## **4- RELATION BETWEEN THE DISPERSION COEFFICIENT AND THE RELATIVE DEPTH**

### **4-1 The 1-D integrated equations**

$$\text{- Continuity : } \frac{\partial(SW)}{\partial z} = m_1 \quad (17)$$

$$\text{- Momentum : } \frac{\partial(\alpha S W W)}{\partial z} = -g S \frac{\partial H}{\partial z} + g S (I - J) \quad (18)$$

$m_1$ : mass flux;

$I$  : The channel slope;

S : Transversal flow section;  
 J : Energy slope;  
 $\alpha$  : Dispersion coefficient.

The dispersion coefficient is computed by the following relation :

$$\alpha = \frac{\langle \overline{W W} \rangle}{\overline{W} \overline{W}} \quad (19)$$

$$\overline{W} = \langle \overline{W} \rangle = \frac{1}{S} \int_s \overline{W} dS \quad \text{is the space averaging.} \quad (20)$$

#### **4.2 Proposed correlation between $\alpha$ and $\beta$**

The computation results confirm that  $\alpha$  is different from the unity and varies as a polynomial function with  $\beta$ . The calculation result provides the following form :

$$\alpha = a + b\beta + c\beta^2 \quad (21)$$

The values of the constants a, b and c are obtained by correlation (figure 14). The final equation is :

$$\alpha = 1.05 + 0.3\beta - 0.66\beta^2 \quad (22)$$

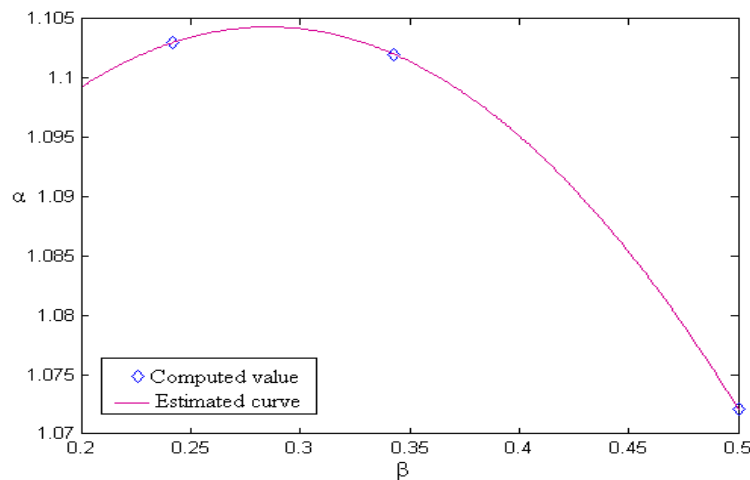


**Figure 14 : Variation of  $\alpha$  with  $\beta$**

### **5- CONCLUSION**

In this work, we have validated the second order turbulence model RSM (Reynolds stress model) for a rectangular compound open channel flow. The numerical results show that the flow structure of the main flow is affected by the secondary currents which expressed the interaction between the main channel and the flood plain (the momentum transfer). This effect is showed by the isovelocity bulging around the main channel and floodplain junction. The flow structure depends on the relative depth  $\beta$  value. Nevertheless, the numerical simulation under-estimate the wall shear stress variation.

Beyond the previous conclusions, the numerical computation of the dispersion coefficient  $\alpha$  allows to express it in function of  $\beta$  with a polynomial relation. An experimental study is necessary to prove this relation.

## **REFERENCES**

- Banjac M. and Vasiljevic B., 2004 – Development of a new near-wall Reynolds Stress Turbulence Model for jet impingement heat transfer prediction. FME Transactions. Vol. 32, N°2, pp. 69-76.
- Cokljat D. and Younis B.A., 1995 – Second-order closure study of open-channel flows. Journal of Hydraulic Engineering, Vol. 121, N° 2, pp. 94–105.
- Knight D.W. and Demetriou J. D., 1983 – Flood plain and main channel flow interaction. Journal of Hydraulic Engineering, Vol. 109, N° 8, pp. 1073-1092.
- Krishnappan B.G. and Lau Y.L., 1986 - Turbulence modelling of floodplain flows. Journal of Hydraulic Engineering, Vol. 112, N° 4, pp. 251-265.
- Launder B.E., Reece G.J. and Rodi W., 1975 – Progress in the development of a Reynolds stress turbulence closure. Journal of Fluid Mechanics, Vol. 68, N°3, pp 537 – 566.
- Myers W.R.C., 1987 – Velocity and discharge in compound channels. Journal of Hydraulic Engineering, Vol. 113, N° 6, pp. 753-767.
- Myers W.R.C., Lyness J.E. and Cassels J., 2001 – Influence of boundary roughness on velocity and discharge in compound river channels. Journal of Hydraulic Research, Vol. 39, N° 3, pp. 311-319.
- Pezzinga G., 1994 - Velocity distribution in compound channel flows by numerical modeling. Journal of Hydraulic Engineering, Vol. 120, N° 10, pp. 1116-1137.
- Schiestel R., 1993 - Modélisation et simulation des écoulements turbulents. Edition HERMES, 505 p.
- Seckin G., 2004 – A comparison of one dimensional methods for estimating discharge capacity of straight compound channels. Canadian Journal of Civil Engineering, Vol. 31, pp. 619-631.
- Shino K. and Knight D.W., 1991 – Turbulent open channel flows with variable depth across the channel. Journal of Fluid Mechanics, Vol. 222, pp. 617-646.
- Sofialidis D. and Prinos P., 1998 – Compound open-channel flow modelling with non-linear low-Reynolds k-ε models. Journal of Hydraulic Engineering, Vol. 124, N° 3, pp. 253–262.
- Tominaga A. , Nezu I. And Izaki K., 1989 – Experimental study on secondary currents in compound open channel flows. Proceeding 23<sup>rd</sup> congress IAHR, Ottawa, Canada, pp A15 – A22.